RSC Advances

ROYAL SOCIETY OF CHEMISTRY

www.rsc.org/advances

Gas collision for improving the precision and accuracy of $^{11}B/^{10}B$ ratios determination in ICP-QMS and its application to determining wine provenance

Wei Guo, Zhiwei Wu, Shenghong Hu*, Lanlan Jin, Keyu Qiu, Qinghai Guo and Yiqun Gan

State Key Laboratory of Biogeology and Environmental Geology, China University of Geosciences, Wuhan, 430074, P. R. China

*Corresponding author. Fax: (+86) 27-67883456; Tel: (+86) 27-67848602.

E-mail address: shhu@cug.edu.cn

Abstract

Boron accumulates with the same isotopic ratio as found in the source soil and water, producing isotope ratios ($^{11}B/^{10}B$) that reflect those of the sources, thus indicating the provenance of products derived from vegetative matter. We developed a simple and valid method based on gas collision inductively coupled plasma quadrupole mass spectrometry (ICP-QMS) for the determination of B isotope ratios to distinguish the geographic origins of wines. Using gas collision technique (using Ne as the collision gas) in ICP-QMS can effectively improve the precision and accuracy of $^{11}B/^{10}B$ determination, which may be due to improvement of the ion transmission or sensitivity (*via* collisional focusing) and a reduction in plasma noise (*via* collisional energy damping). Compared with the conventional method (without Ne gas collision), the precision of the $^{11}B/^{10}B$ ratio was improved 3.2-fold (from 3.15‰ to 0.94‰) and the accuracy was increased from an error of −5.5% to −0.2%. This −0.2% mass bias, resulting from in-cell gas collision, can be accurately corrected using an external bracketing technique with NIST SRM-951 B isotope standard. Direct dilution of the wines by a factor of 100 with 1% HNO_3 was found substantially reduce matrix-induced mass discrimination. Other important parameters such as detector dead time, dwell time per data acquisition, and total integrated time per isotope were also optimised. Twenty wines from nine countries were analysed, with $\delta^{11}B$ values ranged from +1.73 to +46.6‰ with an average external precision (N = 5) of 0.82–1.63‰. The proposed method has sufficient precision to distinguish between 20 wine brands originating from four different geographic regions.

Introduction

Recently, the certification of the authenticity and origin of food products has grown in importance in food markets and to consumer. Wines are no exception, and laws affecting their naming by geographic origin are well-known [1]. Various methods (*i.e.* organic wine components [2], multi-element analysis [3, 4], rare earth element analysis [5], and isotope ratio analysis [6, 7]) based on fingerprinting techniques have been established to guarantee the geographic provenance of wines, and foods in general, to provide additional quality guarantees to the consumer [8, 9]. There are two official European methods for detecting illegal chaptilisation of wine based on measuring the $^{2}H/^{1}H$ ratio by deuterium magnetic resonance spectroscopy (D-MRS) and $\delta^{18}O$ by isotope ratio mass spectrometry (IRMS) [10, 11], however, these methods often required to combine with the data of mutli-element and/or element isotope [12, 13]. A growing number of research articles have been published in last decade detailing the use of elemental concentrations and natural abundance isotope variations as geographic 'tracers' to determine the provenance of agricultural products (such as wine), which due to element composition of agricultural products reflecting the composition of the provenance soil and/or water [8, 9, 14-16]. Certain elements required for plant (*i.e.* grape) growth are taken up by the roots of the vine passing to the grape in the same isotopic proportion as they occur in the soil and/or water [17]. Compared to the isotopic ratios, the composition of absorbed elements (multi-element patterns) are easily affected by some factors, such as production process, soil pH, humidity, porosity, clay, and humic complex *etc* [8].

Isotope techniques are usually classified in two categories: (i) isotope composition of light elements (H, C, N, O, S, *etc.*) and (ii) isotope ratios of heavy elements (Sr, Pb, *etc.*) [8, 14, 18]. In addition, boron isotope ratios ($^{11}B/^{10}B$) could be useful for provenance determination in

agricultural products because B isotopic compositions of soils and/or water can vary in different regions [19-22]. There are two main geochemical processes that affect B isotope composition: (i) ^{11}B enrichment in ocean water, thought to be a result of ^{10}B adsorption on clay and basalt and the low temperature alteration of carbonate minerals and oceanic crust [21-23]; (ii) pH-dependent isotopic exchange (between boric acid, $B(OH)_3$, and the borate ion, $B(OH)_4^-$), which leads to an enrichment of ^{11}B in boric acid [22]. These processes result in isotope abundance variations with $\delta^{11}B$ values of up to 90‰ (from –30 to +60‰) [24], such as –15.9 to +2.2‰ for lake water [25], +14 to +44‰ for groundwater [26], +13.5 to +29.7‰ for vent fluid [27], and –7.5 to +29.3‰ for broccoli and cabbage [28]. In principle, the terrestrial variation in B-isotopic composition should make it possible to use $^{11}B/^{10}B$ ratios to determine the geographical origin of natural products [29]. Distinct $^{11}B/^{10}B$ ratios, with $\delta^{11}B$ values ranging from –11.6 to +36.9‰, were determined in green coffee beans from different geographical locations [20-22].

Thermal ionisation mass spectrometry (TIMS) [21, 22, 30-33] and multi-collector inductively coupled plasma mass spectrometry (MC-ICP-MS) [20, 34-36] are highly precise (<0.05%) and considered to be the best methods for measuring the element isotope ratios. In comparison with these sophisticated MS techniques, quadrupole based ICP -MS (ICP-QMS) has the advantages of low analysis cost, simple operation, instrument robustness, and simple sample preparation, but has low poor precision (0.2–1.0%) [19, 37-41]. Bandura *et al.* reported that collisional damping by a non-reactive gas (Ar or Ne) in a dynamic reaction cell (DRC) resulted in improved precision of Pb and Ag isotope ratios determinations (0.03–0.1%) [42]. They also demonstrated that collisions with non-reactive gas molecules increased the average residence time of the analyte ions in the cell and that ions sampled at slightly different moments in time were actually mixed [42]. As a result, short-term fluctuations in the ion signal intensities were damped and the isotope ratios

precision was improved. This method has been successfully used to improve the precision of Pb [43-46], Se [47], Ca [48, 49] and Fe [50] isotope ratios measurements in tobacco, atmosphere, archaeological artefacts, geological samples, biological samples, snow and sediment. Unlike these heavier elements, lager relative mass differences exist between ^{10}B and ^{11}B (10%), which may influence the precision and accuracy of measured $^{11}B/^{10}B$ ratios due to significant mass discrimination. Therefore, the feasibility of improving the precision of $^{11}B/^{10}B$ ratios using the gas collision ICP-MS method should be carefully evaluated. Total B concentrations in wines from various regions typically range from 5–12 mg L^{-1}, which is sufficiently high to measure isotope ratios using ICP-QMS [19].

The aim of this study was to develop a simple and valid method for determining wine provenance based on B isotope ratios. Using the gas collision technique in the DRC of ICP-MS can effectively improve the precision and accuracy of measured B isotope ratios, which may result from improvements in ion transmission or sensitivity (*via* collisional focusing) and a reduction in plasma noise (*via* collisional energy dampling). The optimised method was applied to the determination of B isotope ratios in 20 different brands of wine originating from nine countries. Differences in B isotope ratios allowed the evaluation of the proposed method as a potential tool for tracing wine provenance.

Experimental

Instrumentation

ICP-MS analysis was performed using a PerkinElmer NEXION 300D ICP-MS instrument. A PFA-400 MicroFlow (self-aspiring, 0.4 mL min^{-1}) nebuliser interfaced with a cyclonic spray

chamber (PC^3 Peltier Chiller) was used with a 2.0 mm i.d quartz injector tube, as described in detail elsewhere [51]. The operating parameters of ICP-MS are summarised in Table 1. Under optimised operating conditions, ^{11}B sensitivity was >20,000 cps/ng mL^{-1}. High purity Ar and Ne gases (99.999% purity) used for ICP-MS were purchased from Praxair Investment Co., Ltd, China.

Reagents and standards

High purity water (18.2 MΩ cm^{-1}), used in the preparation of all standards, blanks, and sample solutions, was produced by a Millipore water purification system (Millipore, France). Nitric acid (HNO_3, 99.9999%), hydrogen peroxide (H_2O_2, 99.999%) and ethanol (>99.9%) were purchased from Alfa Aesar Ltd. (Tianjin, China). The B isotopic standard (1000 mg L^{-1}) was prepared by dissolving 1 g of NIST SRM 951 in 1% (v/v) HNO_3. Working standard solutions were prepared daily by diluting the stock solution with 1% (v/v) HNO_3.

Sampling and sample preparation

Totally twenty red wines of various brands (Table 2) were purchased from different wine stores in China. 25.0 mL of each wine sample added into a 25 ml polypropylene flask and diluted to the scale lines by 1% HNO_3. After above 100-fold dilution, the matrix effects originated from ethanol could be effectively reduced (0.1–0.13 v/v %), meanwhile the concentration of B (35–112 ng mL^{-1}) offered sufficient intensities for B isotope ratio analysis. A microwave digestion method was conducted for comparison: wine (1.0mL), HNO_3 (0.5mL) and H_2O_2 (1.5mL) were added to each digestion bomb and heated for 30 min by increasing the power to 1000 W in a stepwise fashion. The final solution obtained was diluted to 100mL with 1% HNO_3.

Results and discussion

Improvement in $^{11}B/^{10}B$ ratios determination using gas collision technique

Compared with high precision TIMS and MC-ICP-MS, the application of ICP-QMS was advantageous for measuring B isotope ratios due to its low cost, simple operation, and ease of sample preparation. However, poor precision (0.2–1.0% RSD) and poor accuracy (5-10% error) can obtained for $^{11}B/^{10}B$ ratios with traditional ICP-QMS (without a reaction or collision cell) [19, 52, 53], thus making it difficult to distinguish between B sources from different geographical origins. Therefore, efforts were required to improve precision. In this work, a non-reactive gas, Ne, was used as a collision gas in a DRC to improve the precision and accuracy of B isotope ratios measurements. Fig. 1a shows the effect of increasing Ne flow on the average internal precision (the ratio RSD of ten replicates measured five times, with the average of those five RSDs taken) of $^{11}B/^{10}B$ for 100 ng mL^{-1} of NIST SRM 951 standard solution. Under pressurised DRC mode conditions (Ne flow rate = 0.3 mL min^{-1}), the precision (RSD) improved 3.2-fold (from 0.315% to 0.094%), compared with conventional ICP-MS without Ne gas. The theoretical counting statistics errors (SE) and the measured average internal precisions (RSD) as functions of B contents shown in Fig. 2. Using conventional standard mode (without Ne gas collision), the precision of the $^{11}B/^{10}B$ ratios was poorer than its corresponding theoretical counting SE in the range 10–200 ng mL^{-1}. Fortunately, this was improved markedly in the Ne gas collision method; the precision for the gas collision was 0.094% with a corresponding counting SE of 0.091%, whereas for the conventional mode (without Ne) precision was 0.315% and the counting SE 2.2 times larger (Fig. 2). Interestingly, both the signal intensities of ^{11}B and ^{10}B increased up to

three-fold with Ne gas than without Ne gas (Fig. 1b), which may have been due to improvements in ion transmission in the DRC. This phenomenon can be explained as follows: the analyte ions collide with the Ne gas, causing them to lose energy and focus their motion on axis; this collisional energy damping reduces energy spread, while collisional focusing (migration of ions towards the quadrupole axis) results in improved ion transmission and sensitivity [42, 45]. However, the increase in counts (signal intensities) contributed to only a 1.7-fold (square root of 3) improvement in isotope ratio precision. Furthermore, the process of collisional focusing allowed the ions to spend more time in the DRC, reducing short-term signal fluctuations and improving the precision of the isotope ratios determined. This accuracy was important to evaluate the performance of isotope ratio determination. Consequently, the $^{11}B/^{10}B$ isotope ratios (uncorrected values) as a function of Ne gas flow rate shown in Fig. 3. In conventional mode (without Ne), the $^{11}B/^{10}B$ ratio for NIST SRM 951 (100 ng mL^{-1}) was 3.824 with an error of –5.5% relative to the certified value, 4.04362. This large negative error originated from the relative mass difference (10%) between ^{11}B and ^{10}B. Surprisingly, this was minimised using the gas collision technique (Ne = 0.3 mL min^{-1}), in which the $^{11}B/^{10}B$ ratio was 4.040 with an error of –0.1%. Because a high Ne gas flow (>0.6 mL min^{-1}) can cause large collisional scattering and mass discrimination, which leads to poor precision (Fig. 1a) and accuracy (Fig. 3), a low Ne gas flow (0.3 mL min^{-1}) was selected throughput this work. Therefore, a combination of high sensitivity and improved plasma noise by collisional damping resulted in improved precision and accuracy in B isotope ratios.

Optimisation of data acquisition parameters

To obtain the best precision in isotope ratios from ICP-MS, important data acquisition parameters (*e.g.* detector dead time, dwell time per data acquisition and total measurement time per isotope) should be optimised. The detector dead time associated with detector response leads to counting losses that increase in magnitude with increasing counting rate [54]. This, in turn, leads to inconsistencies in isotope abundance ratio measurements that are independent of mass discrimination effects; thus, inconsistencies must be corrected prior to correcting mass discrimination. Equation (1) was used in the determination of the actual counts when applying theoretical dead time values:

$$\frac{1}{C_{obs}} = \frac{1}{C_{act}} + \text{dead time (s)} \qquad (1)$$

Where C_{obs} is the observed count rate (cps) and C_{act} the actual count rate if no detector dead time correction was applied. According to the method of Nelm *et al.* [55], the dead time was determined from where the concentration curves intersected in the graph (Fig. S1, seen ESI†). The obtained dead time value of 64 ns (Fig. S1, seen ESI†) was similar to reported values (53 ns for DRC-e ICP-MS [45] and 61 ns for DRC *plus* ICP-MS [46]). The dwell time and total measurement time per replicate were optimised in Fig. 4. As shown in Fig. 4a, the best precision (0.093% for $^{11}B/^{10}B$) was obtained at dwell time of 2 and 4ms for ^{11}B and ^{10}B, respectively. The optimum total measurement time per replicate was also evaluated by changing the number of sweeps and/or readings from 1 to 1000. As shown in Fig. 4b, when the value was higher than 22s per replicate measurement, no improvement in precision was found. In addition, the optimum replicate number was selected as ten, because precision remained constant between 10 and 20 replicates. Therefore, the total measurement time was 220s per sample. The optimised operation conditions were given in Table 1.

Matrix effects and mass bias correction

The presence of an organic matrix in wine can complicate the analytical performance of $^{11}B/^{10}B$ ratio determination due to the high-count rate at *m/z* 12 resulting from ^{12}C in ethanol and other organic constituents of samples [19, 56]. Therefore, overlap of the ^{11}B peak with the large adjacent ^{12}C peak should be investigated. Fig. 5 shows the normalised $^{11}B/^{10}B$ ratios as a function in 100 ng mL^{-1} B of NIST SRM-951 containing increasing amounts of ethanol. Measurements were conducted with normal-resolution and high-resolution settings. High-resolution settings provided slightly narrower mass spectral peaks, 0.4u instead of 0.7u with 10% of the peak height, and potentially less overlap. Although the $^{11}B/^{10}B$ ratio slightly increased with the ethanol concentration, the results in high-resolution mode were not substantially different to those in normal-resolution mode. According to Fig. 5, if the ethanol concentration was kept below 0.20% (at least 80-fold dilution), the increase in $^{11}B/^{10}B$ ratio was less than 0.15%. Therefore, this potential small contribution from ^{12}C could be corrected by using a corresponding ethanol blank. The results, graphically presented in Fig. 6, of a matrix dilution experiment performed on ZHANGYU wine and a 100 ng mL^{-1} NIST SRM-951 with 12% ethanol, seemed to indicate the presence of a matrix effect. $^{11}B/^{10}B$ ratios systematically decreased with increasing dilution, but appared to level off at higher dilutions. It can therefore be concluded that matrix effects were substantially reduced at 100-fold dilution and that matrix induced mass discrimination was insignificant (<0.1%). Since further dilution would reduce the precision of counting statistics, 100-fold dilution was selected in this study. It is well known that carbon addition (2–5 v/v %) to the plasma enhances (1 to 5–fold) the signal intensity of the high ionisation potential elements (*i.e.* B, As, Se, I, Au, and Hg) [57-61]. However, the observed signal intensity of ^{10}B or ^{11}B was no

difference between a solution of 10 ppb B with addition of 0.15 v/v % ethanol (simulation of real wine after 100-fold dilution) and without addition of ethanol matrix. Therefore, the effects of carbon addition (<0.15 v/v %) could be neglected in this study. Under this 100-fold dilution, the determined $^{11}B/^{10}B$ ratio of a 100 ng mL^{-1} NIST SRM-951 with 12% ethanol was 4.044±0.005, in good agreement with the certified values (4.04362) given by NIST [62]. To further check whether matrix effects caused by the organic matrix of wine could affect measured isotope ratios, the results of microwave digested samples (100-fold dilution) and direct diluted samples (100-fold dilution) are compared in Table 3. There was no difference in the results between the two sample preparation methods, demonstrating that 100-fold dilution adequately reduced matrix effects, thus making it unnecessary to include time-consuming microwave digestion in sample preparation.

Mass discrimination is the bias between the experimental value (after correcting detector dead time and procedure blank) and the corresponding "true" value [54]. Some researchers have reported that the collision gas in the collision/reaction cell affects mass discrimination [45, 46]. Fortunately, the mass bias due to in-cell gas collision can be accurately corrected using the external bracketing technique, because both the samples and isotopic standards are measured under the same conditions [45, 46]. The measurement sequence consisted of a 0.12% ethanol blank, 100 ng mL^{-1} B NIST SRM 951 containing 0.12% ethanol, sample 1, NIST SRM 951 containing 0.12% ethanol, sample 2, NIST SRM 951 containing 0.12% ethanol solution and so on. The obtained B isotope ratios were corrected for mass discrimination by the external bracketing technique and the true sample ratios ($R_{\text{true, sample}}$) were calculated as follows:

$$R_{\text{true,sample}} = R_{\text{NIST,cert}} * \frac{R_{\text{detect,sample}}}{\frac{R_{\text{NIST,before}} + R_{\text{NIST,after}}}{2}} \quad (2)$$

where $R_{\text{NIST, cert}}$ is the certified value of NIST SRM 951 given by NIST [62] and $R_{\text{detect, sample}}$ is the value after the blank correction procedure. B isotope abundance ratios are reported as δ values calculated with respect to NIST SRM-951 (Eq. 3).

$$\delta^{11}\text{B}(‰) = \left[\frac{\left(\frac{^{11}\text{B}}{^{10}\text{B}}\right)_{\text{sample}}}{\left(\frac{^{11}\text{B}}{^{10}\text{B}}\right)_{\text{SRM951}}} - 1\right] \times 1000 \qquad (3)$$

No wine reference material was available, thus, three wines (ZHANGYU, STONEHEDGE, and RAWSON'S RETREAT) were analysed and listed in Table 4. The δ^{11}B values were 14.19±1.16‰, 12.96±1.22‰, and 42.88±0.96‰ for STONEHEDGE, ZHANGYU, and RAWSON'S RETREAT, respectively.

Determining the providence of wine using ^{11}B/^{10}B ratios

Twenty brands of wine from nine countries were measured using the established method. Various brands fell into four distinct categories based on the δ^{11}B values shown in Fig. 7. Each point represents one sample, while the error bars are twice the standard deviation (2SD) of each measurement. The δ^{11}B values ranged from +1.73 to +46.6‰ with average external precisions (N = 5) of 0.82–1.63‰. Fig. 8 shows the literature reported values of +19.9 to +44.6‰ for wines (from EU and South Africa) [19] and –11 to +36.9‰ for green coffee beans [20-22], which were similar with our measured values (+1.73 to +46.6‰). Our determined values of wines for South Africa (+40.2 to +46.6‰) and Italy (+20.7‰) agreed with these of values (+40.2 to +46.6‰ for South Africa and 19.8‰ for Italy) reported by Coetzee and Vanhaecke [19], and the values of South Africa slightly higher than that of values reported by Vorster *et al.* [23] and Santesteban *et*

al. [64] Furthermore, some wines from the USA, China (CHN), South America (SA), Oceania (OA) and Europe (EU) were analysed, as shown in Fig. 7. It can be seen that the δ^{11}B values of wines originating from Africa (AF) and OA (+40.2 to +46.6‰) were markedly higher than those from other regions (<+25.5‰), whereas the δ^{11}B values of wines originating from SA (+1.7 to +7.3‰) were the lowest. Although the δ^{11}B values for wines from CHN and USA (+10.5 to +16.7‰) and EU (+20.7 to +25.6‰) were similar, they could also be discriminated using the δ^{11}B values due to the high precision (~1.63‰). Therefore, the proposed method had sufficient precision and accuracy to distinguish between different wines originating from four different geographic regions.

Conclusions

The established technique is simple, valid, and has sufficient precision to distinguish between the different wine brands originating from four different geographic regions. Further research is necessary to measure a large number of wine samples produced from different regions and to generate a complete geographic database of B isotope ratios to allow the determination of wine provenance and to distinguish counterfeit wines from legal samples.

Acknowledgments

The authors thank Prof. Paul Sylvester (Texas Tech University) for valuable discussion and two anonymous reviewers for their constructive comments. This work was supported by the China Scholarship Council, the National Nature Science Foundation of China (No. 41521001 and No. 21207120), the Ministry of Science and Technology of China (No. 2014DFA20720), the

Fundamental Research Funds for the Central Universities, China University of Geosciences (Wuhan) (No. CUGL140411), and the Research Program of State Key Laboratory of Biogeology and Environmental Geology of China (No. GBL11505).

References

1. S. Marchionni, E. Braschi, S. Tommasini, A. Bollati, F. Cifelli, N. Mulinacci, M. Mattei and S. Conticelli, *J Agri Food Chem*, 2013, **61**, 6822-6831.
2. H. Yu, Y. Zhou, X. Fu, L. Xie and Y. Ying, *Eur Food Res Technol,* 2007, **225**, 313-320.
3. M. J. Baxter, H.M. Crews, M.J. Dennis, I. Goodall and D. Anderson, *Food Chem,* 1997, **60**, 443-450.
4. K. Ariyama, Y. Aoyama, A. Mochizuki, Y. Homura, M. Kadokura and A. Yasui, *J Agric Food Chem*, 2007, **55**, 347-354.
5. E.C. Rossano, Z. Szilagyl, A. Malorni and G. Pocsfalvi, *J Agric Food Chem.*, 2007, **55**, 311-317.
6. S. Marchionni, E. Braschi, S. Tommasini, A. Bollati, F. Cifelli, N. Mulinacci, M. Mattei and S. Conticelli, *J Agric Food Chem*, 2013, **61**, 6822-6831.
7. Y. Zhao, B. Zhang, G. Chen, A. Chen, S. Yang, and Z. Ye, *J Agric Food Chem*, 2013, **61**, 7055-7060.
8. S. Kelly, K. Heaton and J. Hoogewerff, *Trends Food Sci Tech*, 2005, **16**, 555-567.
9. D. M. A. M. Luykx and S. M. van Ruth, *Food Chem*, 2008, **107**, 897-911.
10. Commission Regulation (EEC) No 2348/91. Establishing a databank for the results of analyses of wine products by nuclear magnetic resonance of deuterium. *Official J*, 1991, **L214**, 0039-0043.
11. Commission Regulation (EC) No 1932/97. Amending Regulation (EEC) No 2348/91 Establishing a databank for the results of analyses of wine products by nuclear magnetic resonance of deuterium. *Official J*, 1997, **L272**, 0010-001.
12. G. Gremaud, S. Quaile, U. Piantini, E. Pfammatter and C. Corvi, *Eur Food Res Technol*, 2004, **219**, 97-104.
13. M.P. Day, B. Zhang, G.J. Martin, *J Sci Food Agric*, 1995, **67**, 113-123.
15. C.M. Almeida and M.T. Vasconcelos, *J Agric Food Chem*, 2003, **57**, 4788-4798.
14. S. Holzl, P. Horn, A. Rossmann and S. Rummel, *Anal. Bioanal Chem,* 2004, **378**, 270-272.
16. P.P. Coetzee, L. Greeff and F. Vanhaecke, *S Afr J Enol Vitic*, 2011, **32**, 28-34.
17. C.M. Almeida and M.T. Vasconcelos, *Food Chem* 2004, **85**, 7-12.
18. L. Balcaen, L. Moens and F. Vanhaecke, *SpectrochimActa Part B*, 2010, **65**, 769-786.
19. P. P. Coetzee and F. Vanhaecke, *Anal Bioanal Chem*2005, **383**, 977-984.
20. H. C. Liu, C. F. You, C. Y. Chen, Y. C. Liu and M. T. Chung, *Food Chem*, 2014, **142**, 439-445.
21. F. Serra, C. G. Guillou, F. Reniero, L. Ballarin, M. I. Cantagallo, M. Wieser, S. S. Iyer, K. Heberger and F. Vanhaecke, *Rapid Commun Mass Spectrom*, 2005, **19**, 2111-2115.

22. M. E. Wieser, S. S. Iyer, H. R. Krouse and M. I. Cantagallo, *Appl Geochem*, 2001, **16**, 317-322.
23. C. Vorster, L. Greeff and P.P. Coetzee, *S Afr J Chem.*, 2010, **63**, 207-214.
24. M. R. Palmer and G. H. Swihart, *Rev Mineral*, 1996, **33**, 709-744.
25. A. Vengosh, A. R. Chivas, M. T. Mcculloch, A. Starinsky and Y. Kolodny, *Geochim Cosmochim Acta*, 1991, **55**, 2591-2606.
26. A. Vengosh, A. Starinsky, Y. Kolodny and A. R. Chivas, *J Hydrol*, 1994, **162**, 155-169.
27. K. Yamaoka, E. Hong, T. Ishikawa, T. Gamo and H. Kawahata, *Chem Geol*, 2015, **392**, 9-18.
28. R. A. Vanderpool and P. E. Johnson, *J Agri Food Chem*, 1992, **40**, 462-466.
29. M. Rosner, W. Pritzkow, J. Vorl and S. Voerkelius, *Anal. Chem.*, 2011, **83**, 2562-2568.
30. R. M. Rao, A. R. Parab, K. S. Bhushan and S. K. Aggarwal, *Anal Methods*, 2011, **3**, 322-327.
31. R. M. Rao, A. R. Parab, K. Sasibhushan and S. K. Aggarwal, *Int J Mass Spectrom*, 2009, **285**, 120-125.
32. K. Tirez, W. Brusten, D. Widory, E. Petelet, A. Bregnot, D. M. Xue, P. Boeckx and J. Bronders, *J Anal At Spectrom*, 2010, **25**, 964-974.
33. H. Z. Wei, S. Y. Jiang, Z. Y. Zhu, T. Yang, J. H. Yang, X. Yan, H. P. Wu and T. L. Yang, *Talanta*, 2015, **143**, 302-306.
34. K. Kaczmarek, G. Langer, G. Nehrke, I. Horn, S. Misra, M. Janse and J. Bijma, *Biogeosciences*, 2015, **12**, 1753-1763.
35. S. A. Kasemann, D. N. Schmidt, J. Bijma and G. L. Foster, *Chem Geol*, 2009, **260**, 138-147.
36. L. Lin, Z. C. Hu, L. Yang, W. Zhang, Y. S. Liu, S. Gao and S. H. Hu, *Chem Geol*, 2014, **386**, 22-30.
37. D. L. Callahan, D. J. Hare, D. P. Bishop, P. A. Doble and U. Roessner, *Rsc Adv*, 2016, **6**, 2337-2344.
38. I. G. Tanase, D. E. Popa, G. E. Udristioiu, A. A. Bunaciu and H. Y. Aboul-Enein, *Rsc Adv*, 2015, **5**, 11445-11457.
39. A. S. K. Kumar and S. J. Jiang, *Rsc Adv*, 2015, **5**, 6294-6304.
40. P. Dolcet, A. Mambrini, M. Pedroni, A. Speghini, S. Gialanella, M. Casarin and S. Gross, *Rsc Adv*, 2015, **5**, 16302-16310.
41. I. Takasaki, T. Nagumo, T. Inaba, N. Yoshino and T. Maruyama, *J Nucl Sci Technol*, 2012, **49**, 867-872.
42. D. R. Bandura, V. I. Baranov and S. D. Tanner, *J Anal At Spectrom*, 2000, **15**, 921-928.
43. A. Bazzano and M. Grotti, *J Anal At Spectrom*, 2014, **29**, 926-933.
44. D. De Muynck, C. Cloquet and F. Vanhaecke, *J Anal At Spectrom*, 2008, **23**, 62-71.
45. W. Guo, S. H. Hu, Z. W. Wu, G. Y. Lan, L. L. Jin, X. G. Pang, J. C. Zhan, B. Chen and Z. Y. Tang, *J Anal At Spectrom*, 2015, **30**, 986-993.
46. M. Resano, P. Marzo, J. Pérez-Arantegui, M. Aramendía, C. Cloquet and F. Vanhaecke, *J Anal At Spectrom*, 2008, **23**, 1182-1191.
47. D. Layton-Matthews, M. I. Leybourne, J. M. Peter and S. D. Scott, *J Anal At Spectrom*, 2006, **21**, 41.
48. S. F. Boulyga, U. Klotzli, G. Stingeder and T. Prohaska, *Anal Chem*, 2007, **79**, 7753-7760.
49. S. Stürup, L. Bendahl and B. Gammelgaard, *J Anal At Spectrom*, 2006, **21**, 297-304.
50. F. Vanhaecke, L. Balcaen, G. N. De Wannemacker and L. Moens, *J Anal At Spectrom*, 2002, **17**, 933-943.

51. W. Guo, W. Xie, L. Jin, Q. Guo and S. Hu, *RSC Adv.*, 2015, **5**, 103189-103194.
52. A. Al-Ammar, E. Reitznerova and R. M. Barnes, *Spectrochim Acta Part B*, 2000, **55**, 1861-1867.
53. F. Vanhaecke, G. de Wannemacker, L. Moens and J. Hertogen, *J Anal At Spectrom*, 1999, **14**, 1691–1696.
54. R. Santos, M. J. Canto Machado, I. Ruiz, K. Sato and M. T. S. D. Vasconcelos, *J Anal At Spectrom*, 2007, **22**, 783.
55. S. M. Nelms, C. R. Quetel, T. Prohaska, J. Vogl and P. D. P. Taylor, *J Anal At Spectrom*, 2001, **16**, 333-338.
56. J. Vogl, M. Rosner and W. Pritzkow, *J Anal At Spectrom*, 2011, **26**, 861.
57. D. Fliegel, C. Frei, G. Fontaine, Z. C. Hu, S. Gao and D. Gunther, *Analyst*, 2011, **136**, 4925-4934.
58. W. Guo, W. K. Xie, L. L. Jin, Q. H. Guo and S. H. Hu, *RSC Adv*., 2015, **5**, 103189-103194.
59. W. Guo, Y. X. Wang, J. X. Li, Y. Peng, L. L. Jin, Q. H. Guo and S. H. Hu, *Atom Spectrosc*, 2016, 37, 7-12.
60. W. Guo, S. H. Hu, Y. X. Wang, L. Y. Zhang, Z. C. Hu and J. Y. Zhang, *Microchem J* , 2013, **108**, 106-112.
61. W. Guo, S. H. Hu, J. Y. Zhang, L. L. Jin, X. J. Wang, Z. L. Zhu and H. F. Zhang, *J Anal At Spectrom*, 2011, **26**, 2796-2780.
62. US National Institute of Standards and Technology (NIST), https://www-s.nist.gov/srmors/certificates/archive/951.Feb28,%201969.pdf.
63. Q. L. Xie and R. Kerrich, *J Anal At Spectrom*, 2002, **17**, 69-74.
64. L.G. Santesteban, C. Miranda, I. Barbarin and J.B. Royo, *Aust J Grape Wine R*, 2015, **21**, 157-167.42.

Graphic Abstract: *Gas collision for improving the precision and accuracy of $^{11}B/^{10}B$ ratios determination in ICP-QMS*

Figure captions

Fig.1 (a) Average internal precision RSD (%) of $^{11}B/^{10}B$ ratios (N = 5, replicate = 10) and (b) signal intensities of ^{11}B and ^{10}B as functions of Ne collision gas flow rate.

Fig.2 Measured precision and theoretical counting statistics errors (SE) of $^{11}B/^{10}B$ ratios with and without Ne gas collision as a function of B contents.

Fig.3 The effect of Ne collision gas flow rate on uncorrected of $^{11}B/^{10}B$ ratio data.

Fig.4 Optimisation of (a) the dwell time per acquisition point and (b) the total measurement time per replicate for B isotopic ratios in a 100 ng mL^{-1} NIST SRM 981 B standard solution by ICP-QMS with a 0.3 mL min^{-1} of Ne as the collision gas.

Fig.5 Normalised $^{11}B/^{10}B$ ratios using normal-resolution (0.7u) and high-resolution (0.4u) settings as a function of different amounts of ethanol in a 100 ng mL^{-1} NIST SRM 981 B standard solution.

Fig.6 Effects of dilution factors on the $^{11}B/^{10}B$ ratio of a real wine (ZHANGYU) and a 100 ng mL^{-1} NIST SRM-951 solution with 12% ethanol matrix.

Fig.7 $\delta^{11}B$ values for 20 different brands of wine originating from nine different countries. AF, OA, EU, CHN, US, SA are represented the wine samples from Africa, Oceania, Europe, China, America, South America, respectively.

411 **Fig. 8** δ^{11}B values for plants reported in the literatures [19-22].

412

413

Tables

Table 1 Instrument operating parameters

ICP-MS instrument	Perkin-Elmer NEXION 300D
Sample introduction	PFA-400 MicroFlow nebuliser (self-aspiring)
Spray chamber	Cyclonic spray chamber (PC^3 Peltier Chiller)
Injector tube	2.0 mm id Quartz
RF power, W	1550
Plasma gas flow, L min^{-1}	15
Auxiliary gas flow, L min^{-1}	1.00
Nebuliser gas flow, L min^{-1}	0.80
Lens Voltage, V	8.0
Autolens	Off
DRC parameters	
Cell gas Ne, mL min^{-1}	0.30
Rejection parameter, q	0.5
Rejection parameter, a	0
QRO	−6
CRO	−1
CPV	−15
Data acquisition parameters	
Scanning mode	Peak hopping
Detector mode	Pulse counting
Detector dead time, ns	62
Dwell time, ms	2 for $^{11}B^+$ and 4 for $^{10}B^+$
Settling time, µs	200

Sweeps	1000
Readings	3
Replicates	10
Total analysis time, s	220

416

417

418

419 **Table 2** Descriptions of twenty red wines and their origin.

Sample No.	Brands	Country of origin	Sample No.	Brands	Country of origin
1	VINALBA MALBEC	Argentina	11	MOUNTAIN RANGE	Chile
2	TRIVENTO	Argentina	12	RESERVADO	Chile
3	STONEHEDGE	USA	13	VILLA	Italy
4	SHANGRI-LA	China	14	KESSLER-ZINK	Germany
5	GREATWALL-1	China	15	LAFITE	France
6	GREATWALL-2	China	16	JACOB'S CREEK	Australia
7	ZHANGYU	China	17	RAWSON' S RETREAT	Australia
8	MOGAO	China	18	ARABELLA-1	South Africa
9	FENGSHOU	China	19	ARABELLA-2	South Africa
10	NIYA	China	20	KUMALA	South Africa

420

421 **Table 3** Comparison of $^{11}B/^{10}B$ ratios obtained from direct diluted samples and digested samples (n=5).

Sample	$^{11}B/^{10}B$		
	Direct diluted (±SD)	Microwave digested (±SD)	Certified values (±SD) [63]
NIST SRM-951 with 12% ethanol	4.044±0.005	4.043±0.006	4.04362±0.00137
STONEHEDGE wine	4.101±0.007	4.103±0.008	/
ZHANGYU wine	4.096±0.006	4.094±0.006	/
RAWSON'S RETREAT wine	4.217±0.006	4.215±0.007	/

422 SD represents one standard deviation.

423

424

425

426 **Table 4** Results of $\delta^{11}B$ for three wine samples (n=5)

Wines	$\delta^{11}B$		
	Measured values (±2-fold standard deviation)	Internal precision (‰)	External precision (‰)
STONEHEDGE	14.19±1.16	1.02	0.58
ZHANGYU	12.95±1.22	0.97	0.61
RAWSON'S RETREAT	42.88±0.96	0.98	0.48

427

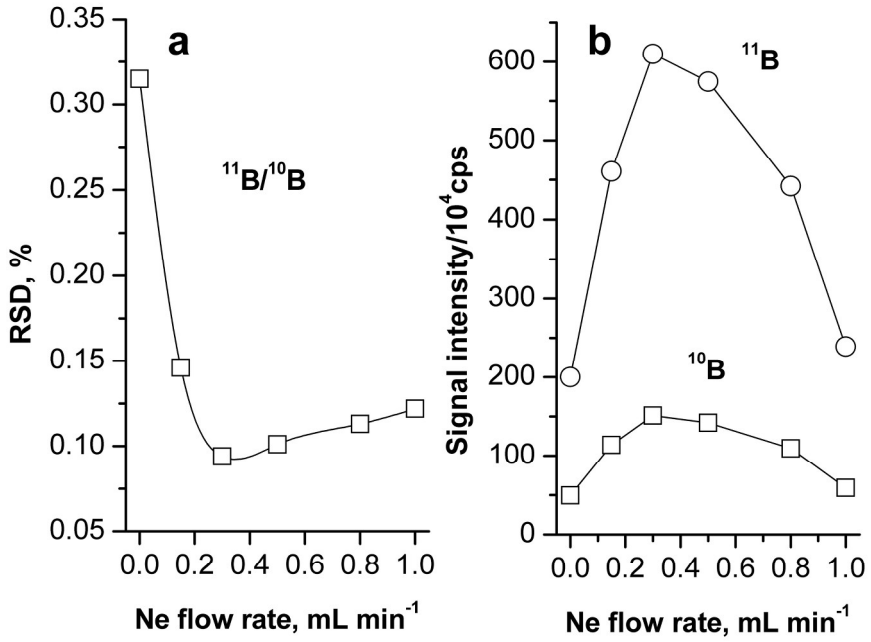

Fig.1 (a) Average internal precision RSD (%) of $^{11}B/^{10}B$ ratios (N = 5, replicate = 10) and (b) signal intensities of ^{11}B and ^{11}B as functions of Ne collision gas flow rate.
210x148mm (300 x 300 DPI)

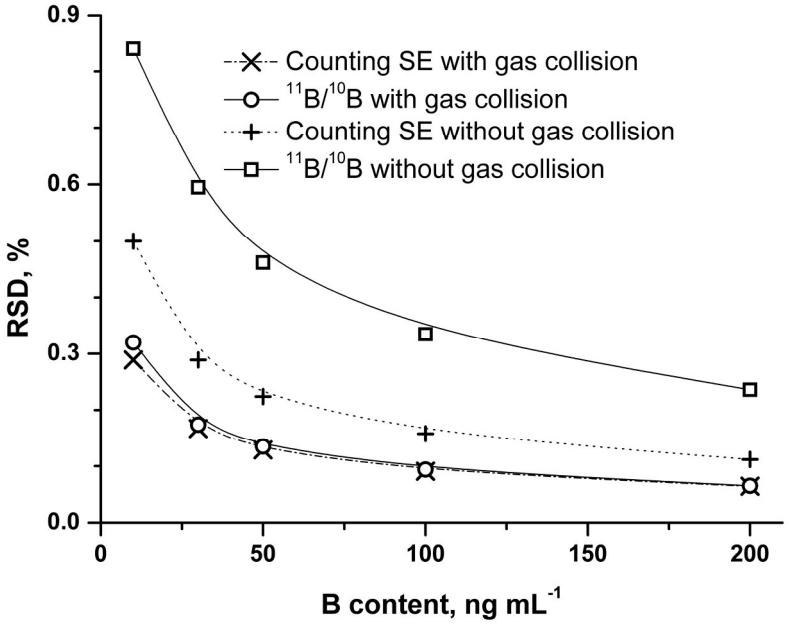

Fig.2 Measured precision and theoretical counting statistics errors (SE) of $^{11}B/^{10}B$ ratios with and without Ne gas collision as a function of B contents.
210x148mm (300 x 300 DPI)

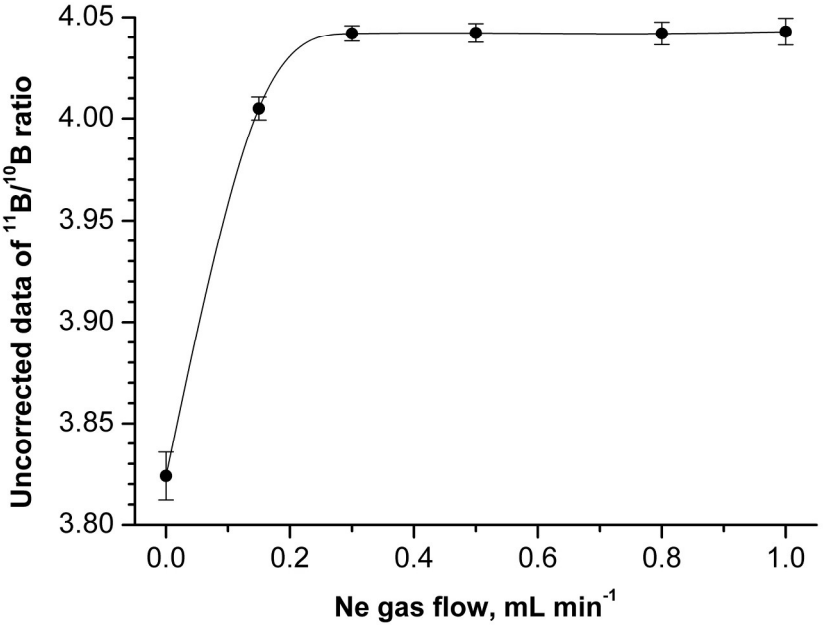

Fig.3 The effect of Ne collision gas flow rate on uncorrected of $^{11}B/^{10}B$ ratio data.
210x148mm (300 x 300 DPI)

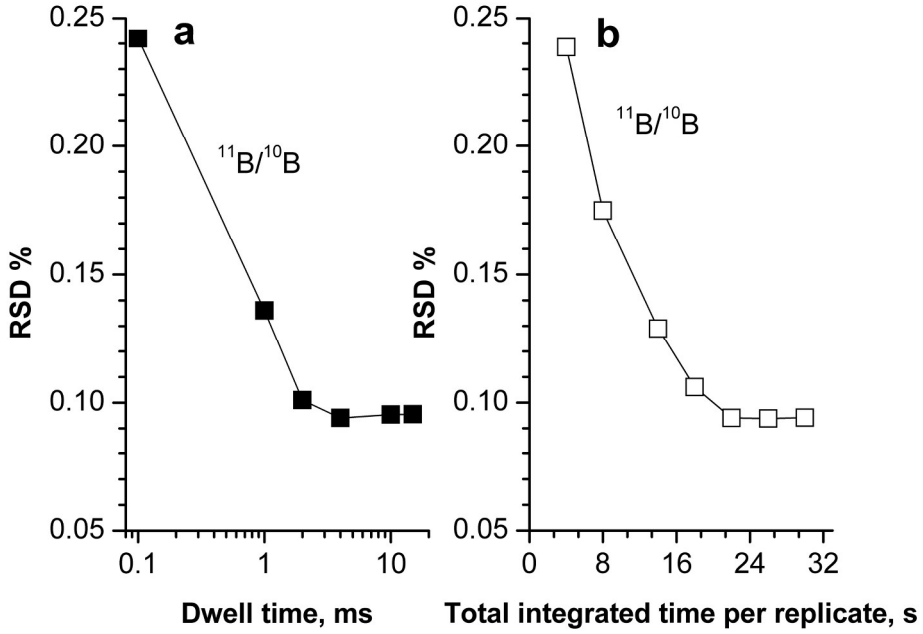

Fig.4 Optimisation of (a) the dwell time per acquisition point and (b) the total measurement time per replicate for B isotopic ratios in a 100 ng mL^{-1} NIST SRM 981 B standard solution by ICP-QMS with a 0.3 mL min^{-1} of Ne as the collision gas.
210x148mm (300 x 300 DPI)

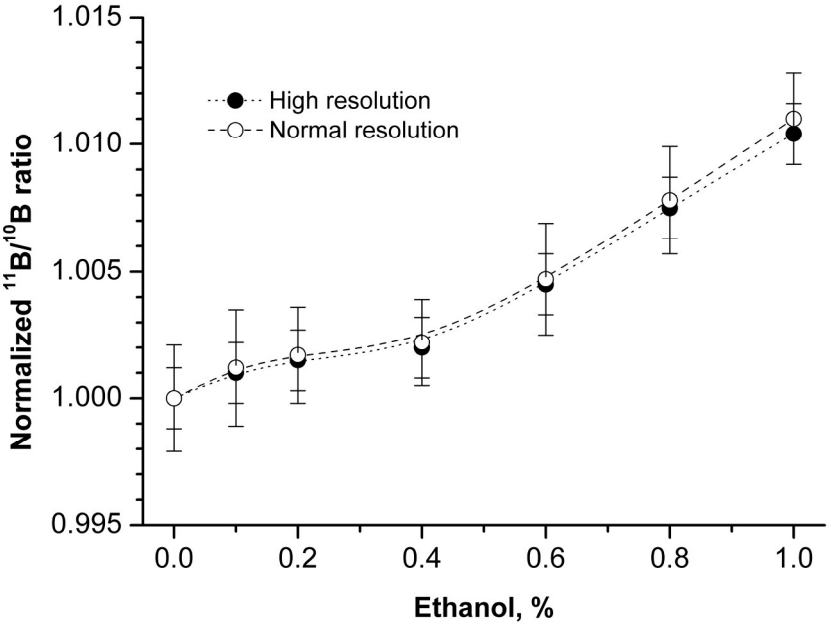

Fig.5 Normalised $^{11}B/^{10}B$ ratios using normal-resolution (0.7u) and high-resolution (0.4u) settings as a function of different amounts of ethanol in a 100 ng mL^{-1} NIST SRM 981 B standard solution.
210x148mm (300 x 300 DPI)

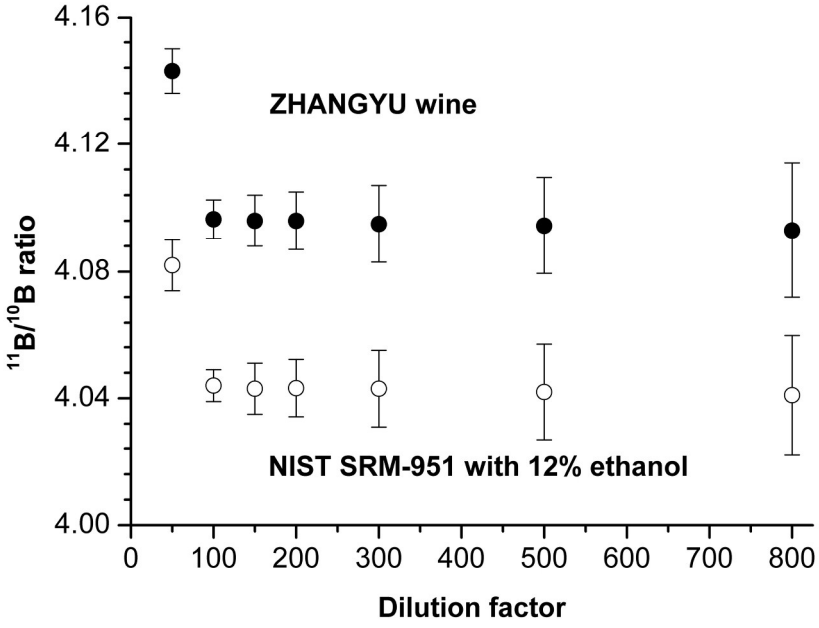

Fig.6 Effects of dilution factors on the $^{11}B/^{10}B$ ratio of a real wine (ZHANGYU) and a 100 ng mL^{-1} NIST SRM-951 solution with 12% ethanol matrix.
210x148mm (300 x 300 DPI)

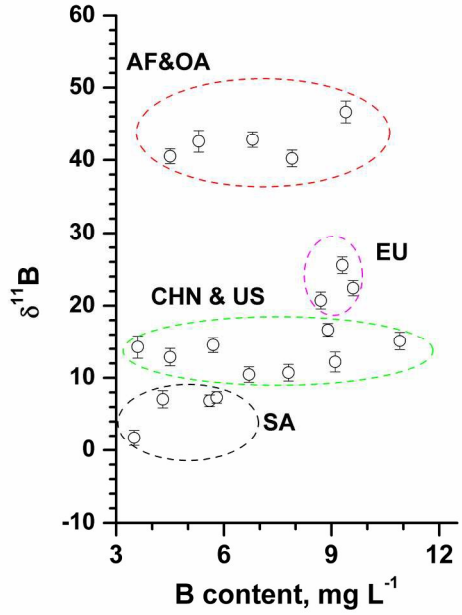

Fig.7 δ^{11}B values for 20 different brands of wine originating from nine different countries. AF, OA, EU, CHN, US, SA are represented the wine samples from Africa, Oceania, Europe, China, America, South America, respectively.
210x148mm (300 x 300 DPI)

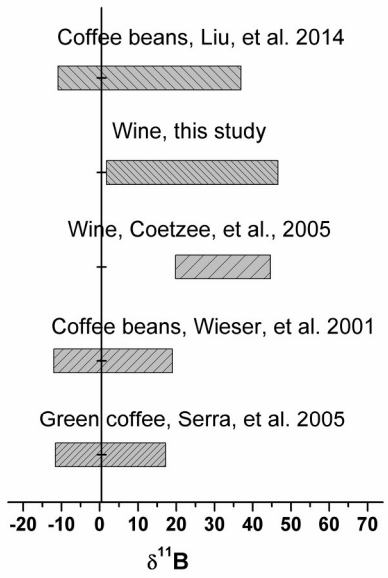

Fig. 8 $\delta^{11}B$ values for plants reported in the literatures [19-22].
210x148mm (300 x 300 DPI)

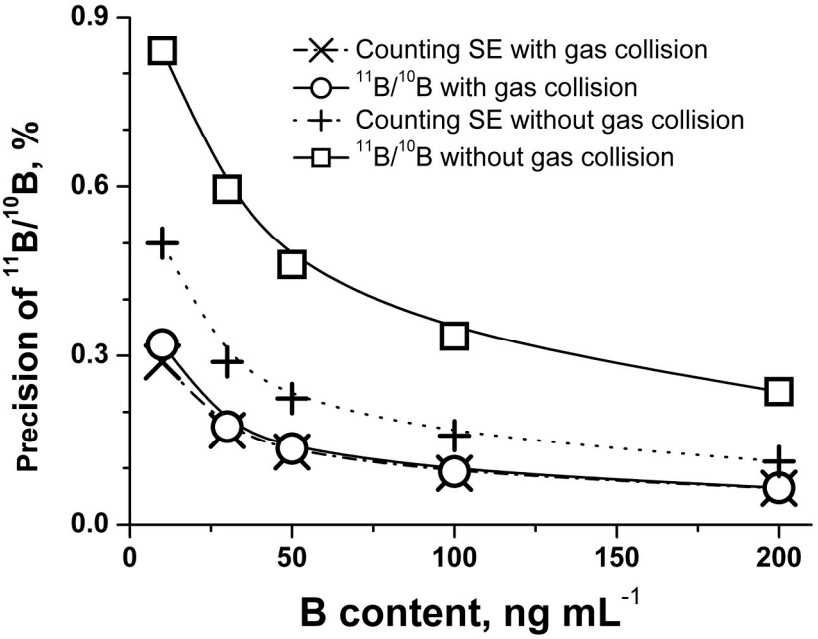

210x148mm (300 x 300 DPI)